Neuron, Vol. 32, 841–853, December 6, 2001, Copyright ©2001 by Cell Press

Heteromeric AMPA Receptors Assemble with a Preferred Subunit Stoichiometry and Spatial Arrangement

Michael Mansour,[1] Naveen Nagarajan,[1] Ralf B. Nehring,[1] John D. Clements,[2] and Christian Rosenmund[1,3]
[1]Department of Membrane Biophysics
Max-Planck-Institute for Biophysical Chemistry
D-37070 Goettingen
Germany
[2]Division of Biochemistry and Molecular Biology
Australian National University
Canberra ACT 0200
Australia

Summary

AMPA receptors are thought to be a tetrameric assembly of the subunits GluR1-4. We have examined whether two coexpressed subunits (GluR1/2) combine at random to form channels, or preferentially assemble with a specific stoichiometry and spatial configuration. The subunits carried markers controlling ion permeation and desensitization, and these properties were monitored as a function of relative expression level and subunit composition. Homomeric receptors assembled stochastically while heteromeric receptors preferentially formed with a stoichiometry of two GluR1 and two GluR2 subunits, and with identical subunits positioned on opposite sides of the channel pore. This structure will predominate if GluR1 binds to GluR2 more rapidly during receptor assembly than other subunit combinations. The practical outcome of selective heteromeric assembly is a more homogenous receptor population in vivo.

Introduction

Ionotropic glutamate receptors of the AMPA subtype are multisubunit ligand-gated ion channels that mediate the majority of fast excitatory synaptic responses in the CNS (Dingledine et al., 1999). Channel properties are actively controlled by various genetic mechanisms including tissue- and developmental-specific subunit expression, and RNA splicing and editing. For example, in the auditory system where signal transmission requires submillisecond accuracy for sound localization, low affinity, rapidly desensitizing AMPA receptors are preferentially expressed (Raman et al., 1994; Trussell, 1999).

Another important mechanism that controls AMPA receptor function is heteromerization. Recent studies suggest that AMPA receptors form as a tetramer of subunits (Mano and Teichberg, 1998; Rosenmund et al., 1998). Four cloned subunits (GluR1-4) have been characterized in detail. In vivo, most AMPA receptors are a coassembly of the subunits GluR2 with GluR1, 3, or 4 (Jonas and Burnashev, 1995). This serves to control the permeation and kinetic properties of the channel. Among the AMPA receptor subunits, only GluR2 receptors are edited from a glutamine residue to an arginine at position 607 (Q/R site) in the M2 reentrant loop (Seeburg et al., 1998). Homomeric $GluR2_R$-edited receptors form low conductance channels that are calcium impermeable (Burnashev et al., 1992), while homomeric expression of the Q-containing (GluR1, 3, or 4) receptor subunits yields high conductance channels, which are calcium permeable, and are also inwardly rectifying due to pronounced block of outward current by intracellular polyamines (Jonas and Burnashev, 1995; Bowie and Mayer, 1995; Donevan and Rogawski, 1995). Coexpression of $GluR2_R$ with GluR1, 3, or 4 conjugates the biophysical properties of the homomers. The resulting channels have a high conductance, low permeability to calcium, and have an approximately linear current-voltage (I-V) relationship (Verdoorn et al., 1991; Hume et al., 1991; Washburn et al., 1997), suggesting that the majority assemble as heteromers. They exhibit reduced calcium permeability, even when the relative expression of $GluR2_R$ is low. Most native AMPA channels are also calcium impermeable and nonrectifying (Geiger et al., 1995; Washburn et al., 1997; Iino et al., 1994), and immunoprecipitation reveals that receptors from CA1/CA2 hippocampal pyramidal neurons are predominantly GluR2/1 or GluR2/3 heteromers (Wenthold et al., 1996). These findings suggest that heteromeric channels assemble efficiently, and that inclusion of a single $GluR2_R$ subunit is sufficient to reduce calcium permeability (Geiger et al., 1995; Washburn et al., 1997). However, interpretation of these results requires simplifying assumptions about the subunit assembly process. It remains unclear whether subunits combine randomly, or whether specific mechanisms exist that promote the preferential assembly of heteromeric channels incorporating GluR2. Furthermore, it is not known whether the spatial arrangement of subunits within the oligomer affects channel function.

In the present study, we explored the structural and functional interaction of subunits in homomeric and heteromeric GluR1 and GluR2 receptor channels. Our results suggest that both permeability and desensitization of AMPA receptors are sensitive to the spatial configuration of the receptor subunits. Furthermore, coassembly of GluR1 and GluR2 involves intersubunit interactions that favor a symmetric configuration, with two GluR2 subunits positioned on opposite sides of the channel pore.

Results

Different Pattern of Marker Expression for Homomeric and Heteromeric AMPA Receptors

We introduced two independent point mutations (markers) into GluR1 and GluR2 subunits to investigate how they assemble. Each mutation alters a functional property of the assembled AMPA channel (marker phenotype). Marked GluR subunits were coexpressed with unmarked subunits, and the fraction of channels expressing the marker phenotype was monitored. The two markers were used separately and in combination,

[3]Correspondence: crosenm@gwdg.de

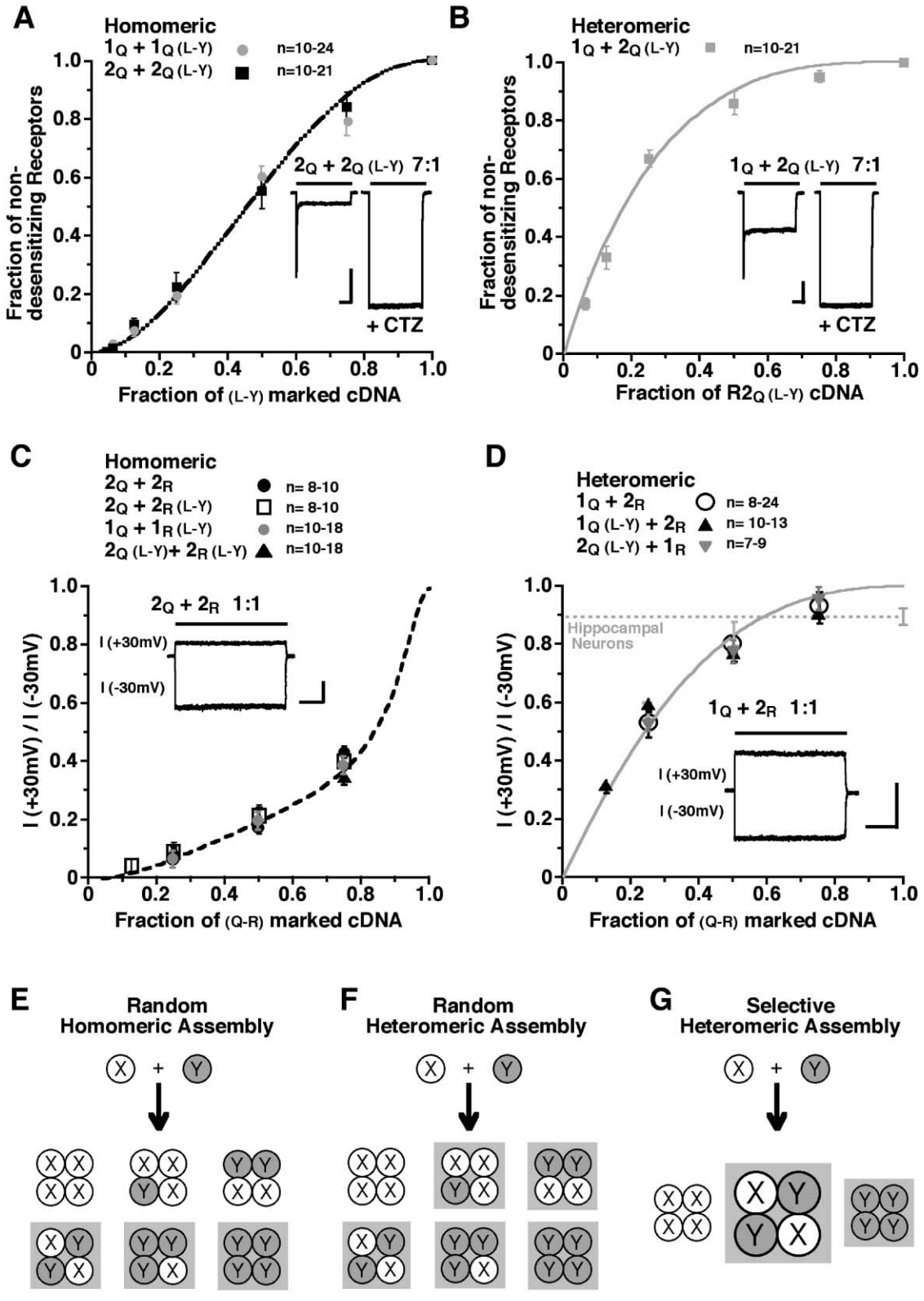

Figure 1. Marker Phenotype Expression Is Different for Homomeric and Heteromeric Receptors

(A) Summary of results from homomeric $1_Q + 1_Q$(L-Y) and $2_Q + 2_Q$(L-Y) cotransfection experiments. The nondesensitization index (steady-state current in the absence of cyclothiazide/steady-state current in the presence of cyclothiazide) is plotted against the fraction of DNA carrying the nondesensitizing L-Y marker. n is the number of outside-out patches. A theoretical fit is superimposed to aid comparison with other panels (dashed line). Inset, current evoked by 10 mM glutamate (black bar) in an outside-out patch excised from an HEK cell cotransfected

which provided internal controls on the reliability of the data and permitted crosschecking of the results.

Mutation of a highly conserved leucine residue in the extracellular ligand binding domain (GluR1 L497; GluR2 L504; GluR3 L507) to aromatic residues yields receptors that are completely nondesensitizing (Stern-Bach et al., 1998; Thalhammer et al., 1999; Takamori et al., 2000; Robert et al., 2001). In this study, a tyrosine point mutation (L→Y) was used as a marker, and the amount of desensitization indicated the fraction of receptors that expressed the marker phenotype. A typical result is shown in Figure 1A, inset. Homomeric $GluR2_Q$ (abbreviated as 2_Q) and $GluR2_Q$ L504Y (abbreviated as 2_Q(L-Y)) subunits were cotransfected into HEK cells at a DNA ratio of 7:1, and recordings were obtained from outside-out patches using a fast application system (Rosenmund et al., 1998). The response to a saturating pulse of glutamate was measured in the absence and presence of cyclothiazide. As expected, the inclusion of nondesensitizing receptor subunits (12.5%) led to a small nondesensitizing component of the response (Figure 1A, inset). However, when heteromeric 1_Q and 2_Q(L-Y) subunits were cotransfected at the same 7:1 ratio, the nondesensitizing component was much larger (Figure 1B, inset). Clearly, there is a difference in nondesensitization phenotype expression between homomeric and heteromeric receptors.

The response in the presence of cyclothiazide (Figure 1A, inset) is a measure of the total receptor population because it blocks desensitization of wild-type receptors while leaving nondesensitizing responses unaffected (Stern-Bach et al., 1998). The steady-state response in the absence of cyclothiazide divided by the response in the presence of cyclothiazide (nondesensitization index) was used to quantify the fraction of receptors expressing the nondesensitizing marker phenotype. The ratio of marked and unmarked subunit DNA was systematically altered in a series of cotransfections, and the phenotype expression index was plotted against the fraction of marked subunits. The nondesensitization index was larger for heteromeric receptors (Figure 1B) than homomeric receptors (Figure 1A) at all subunit ratios. The difference in marker phenotype expression was greatest when the fraction of marked subunits was <0.5. Thus, nondesensitizing heteromeric AMPA receptors assemble more readily than nondesensitizing homomeric receptors. This could be due to a difference in subunit assembly, or in the pattern of phenotype dominance. To investigate this further, we repeated the experiment using a second, independent marker.

Ion permeation through AMPA receptors is controlled by the presence of an arginine/glutamine in the pore-forming second transmembrane domain. The presence of the edited version of the GluR2 subunit (Q607R) in the assembled channel abolishes rectification. In the absence of a 2_R subunit, channels are inwardly rectifying due to intracellular spermine block (Burnashev et al., 1992; Bowie and Mayer, 1995; Donevan and Rogawski, 1995; Kamboj et al., 1995; Koh et al., 1995). A point mutation (Q→R), which mimicked post-translation editing, was used as a second marker. The amount of inward rectification was monitored to assess the percentage of receptors that expressed the marker phenotype. Typical results are shown for coexpression of homomeric subunits 2_Q and 2_R at a ratio of 1:1 (Figure 1C, inset), and for coexpression of the heteromeric subunits 1_Q and 2_R at a ratio of 1:1 (Figure 1D, inset). The current amplitude was measured at -30 mV and $+30$ mV with 50 μM spermine in the recording pipette and cyclothiazide in the extracellular solution. The ratio of outward current to inward current (nonrectification index) was used to quantify the fraction of receptors expressing the marker phenotype. The nonrectification index was much larger for heteromeric coexpression (0.80 ± 0.03, $n = 24$) than for homomeric coexpression (0.2 ± 0.05, $n = 12$, $p < 0.05$), implying that nonrectifying heteromeric receptors assemble more readily than nonrectifying homomeric receptors. To further investigate the pattern of marker phenotype expression, seven different subunit combinations were tested, and the ratio of marked and unmarked subunit DNA was systematically varied. The results were very consistent. The nonrectification index was always larger for heteromeric receptors (Figure 1D) than homomeric receptors (Figure 1C). Interestingly, the nonrectification index of heteromeric channels at a 1:1 subunit ratio was similar to results from AMPARs in principal neurons of hippocampus and neocortex (Colquhoun et al., 1992; Jonas et al., 1994; Geiger et al., 1995) (Figure 1D).

The results in Figures 1A–1D clearly demonstrate that both marker phenotypes are expressed much more readily by heteromers than by homomers. There are two alternative explanations. It is possible that both homomeric and heteromeric receptors assemble randomly, but more of the heteromeric subunit configurations express the marker phenotype (Figures 1E and 1F). This

with $2_Q + 2_Q$(L-Y) at a ratio of 7:1. The experiment was repeated in the continuous presence of 100 μM cyclothiazide (+CTZ). All scale bars are 200 ms, 50 pA. All error bars represent standard error of mean.

(B) Summary of results from heteromeric $1_Q + 2_Q$(L-Y) cotransfection experiments. The nondesensitization index is plotted against the fraction of 2_Q(L-Y) cDNA. Inset: typical response following cotransfection with heteromeric $1_Q + 2_Q$(L-Y) at a ratio of 7:1. Currents were evoked as in (A).

(C) Summary of homomeric $2_Q + 2_R$, $2_Q + 2_R$(L-Y), $1_Q + 1_R$(L-Y), and 2_Q(L-Y) + 2_R(L-Y) cotransfection experiments. The nonrectification index (steady-state current at +30 mV/steady-state current at −30 mV) is plotted against the fraction of DNA carrying the nonrectifying Q-R marker. Inset: currents evoked by 10 mM glutamate (black bar) at −30 mV and +30 mV in the continuous presence of 100 μM cyclothiazide, following cotransfection with $2_Q + 2_R$ at a ratio of 1:1.

(D) Summary of heteromeric $1_Q + 2_R$, 1_Q(L-Y) + 2_R and 2_Q(L-Y) + 1_R cotransfection experiments. The nonrectification index is plotted against the fraction of Q-R marked cDNA. Inset: typical response following cotransfection with $1_Q + 2_R$ at a ratio of 1:1. Currents were evoked as in (C). Dotted horizontal line indicates mean ± SEM of nonrectification index obtained from primary hippocampal neurons ($n = 13$).

(E) Wild-type (X) and marked (Y) homomeric subunits assemble randomly into the six possible configurations. A subset of the configurations express the marker phenotype (3 shaded boxes).

(F) If heteromeric subunits assemble randomly, then more subunit combinations must express the marker phenotype (5 shaded boxes).

(G) Alternatively, heteromeric subunits may preferentially assemble into a configuration that expresses the marker phenotype (large shaded box).

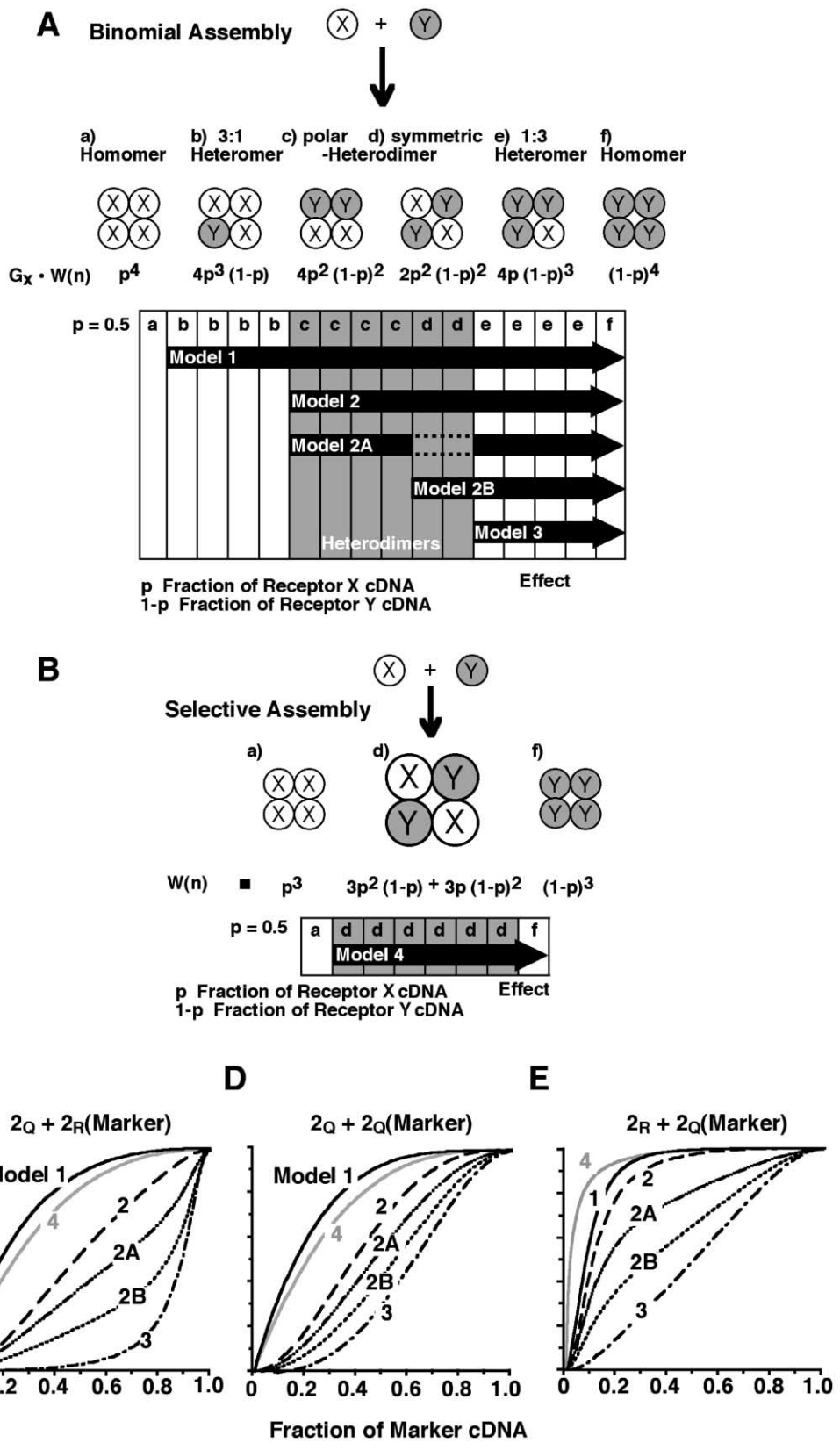

Figure 2. Phenotype Expression Models

(A) Binomial assembly. When two different subunits, X and Y, assemble stochastically, the frequency of the various subunit combinations follows a binomial distribution. There are 16 possible tetrameric assemblies, shown schematically as 16 vertical columns, but there are only 6 distinct subunit configurations (a–f). Subunit Y (shaded) carries a marker mutation. An arrow indicates which subunit configurations express

explanation is counterintuitive because it implies that substituting an unmarked GluR2 subunit with an unmarked GluR1 subunit can change the marker phenotype. It also requires that the substitution affects both L→Y and Q→R phenotypes in the same way, so this explanation appears unlikely. A simpler explanation is that heteromeric subunits preferentially combine in a particular configuration that expresses both the L→Y and Q→R phenotypes (selective assembly, Figure 1G). Consistent with this hypothesis, the pattern of heteromeric phenotype expression is very similar for both markers (Figures 1B and 1D). To rigorously distinguish between these two hypotheses, we developed quantitative models of subunit assembly and phenotype dominance.

A Model of GluR Subunit Assembly

We developed two models of AMPA receptor assembly and phenotype dominance, one based on random GluR subunit assembly and the other on selective assembly. These models were used to investigate the difference between homomeric and heteromeric phenotype expression, and to determine which of the homomeric subunit configurations express the marker phenotypes.

The AMPA receptor is thought to be a tetramer (Rosenmund et al., 1998; Mano and Teichberg, 1998), so its subunits have six possible spatial configurations (Figure 2A). Homomeric receptors are assumed to assemble in a stochastic fashion since the marked and unmarked subunits have an almost identical structure. The percentage of receptors that will assemble into each of the six configurations can be calculated from the binomial distribution, $w(n) = \Sigma p^n(1-p)^{n-1}$ (Figure 2A). Note that two subclasses of 2:2 heterodimers exist based on the geometric configuration of the subunits within the receptor. One subclass has "specific point symmetry" (identical subunits located on opposite sides of the channel pore, Figure 2Ad), and the other subclass is "polar" (identical subunits are side by side, Figure 2Ac).

In contrast to homomeric receptors, the assembly of heteromeric receptors may not be random. Interactions between GluR1 and GluR2 may favor the assembly of particular subunit configurations. We have chosen a simple model where only point symmetric subunit configurations are assembled. This again leads to a binomial distribution of the three permitted configurations (Figure 2B).

If we assume that each subunit configuration expresses either the wild-type or the marker phenotype (no intermediate phenotypes), then the assembly models can be used to predict the total fraction of channels that express the marker phenotype. We developed a series of phenotype expression models, each of which assigns the marker phenotype to a different subset of the six possible subunit configurations (Figure 2A). Model 1 assumes that the inclusion of one or more marked subunits is sufficient to convert the phenotype of the assembled channel. In Model 2, it is assumed that the channel is converted to the marker phenotype when two or more marked subunits are present: in Model 2A, when two marked subunits are present side by side (polar heterodimer); in Model 2B when two marked subunits are located on opposite sides of the channel pore (specific point symmetry); and in Model 3 when three or more marked subunits are present. The situation is simpler for selective assembly (Figure 2B). Model 4 assumes that only symmetric assemblies are permitted, and that two or more marked subunits convert the channel phenotype.

The model predictions depend on the channel conductances of the various subunit combinations. Where necessary, the phenotype expression models incorporate the average conductance for each subunit configuration, normalized to the 1_Q conductance. These conductance parameters were estimated from single channel and variance-mean experiments (see Experimental Procedures). The normalized conductance was set to 1.7 for 2_Q homomers, 0.8 for $1_Q/2_R$ 3:1 and 2:2 heteromers, and 1.3 for $1_Q/2_Q$ 3:1 and 2:2 heteromers. It is known that 2_R homomers conduct relatively little current (Swanson et al., 1997), so the normalized conductance was set to 0.05 for 2_R homomers, 0.05 for $1_Q/2_R$ 1:3 heteromers, and 0.085 for $2_Q/2_R$ 1:3 heteromers. The relationship between the marker phenotype expression and fraction of marked subunits predicted by Models 1–3 is shown for coexpression of $2_Q + 2_R$(marker), $2_Q + 2_Q$(marker), and $2_R + 2_Q$(marker) (Figures 2C–2E).

The assumptions underlying the phenotype expression models are well supported by an extensive series of control experiments. We confirmed that subunit expression is linearly related to the amount of cDNA used in the transfection using two independent approaches (see Experimental Procedures). We also tested the assumption that each receptor configuration expresses either the wild-type or marker phenotype. Subunits carrying both L→Y and Q→R markers were coexpressed with wild-type subunits. The amount of desensitization was observed at positive and negative potentials, providing a sensitive test for intermediate phenotypes (see Supplementary Figure S1 at www.neuron.org/cgi/content/full/32/5/841/DC1). We also examined the time course of desensitization in search of a component with an intermediate time constant (see Supplementary Figure S1 on *Neuron* website). The results support the model assumptions. In addition to these direct tests, the excellent agreement between model predictions and

the marker phenotype in each model. The 2X:2Y heteromeric assemblies (c and d) are shown in gray. There is a polar form (c) and a point symmetric form (d).

(B) Selective assembly. Interactions between GluR1 and GluR2 may destabilize asymmetric subunit configurations. A binomial assembly model predicts the frequency of the three symmetric configurations. Phenotype expression Model 4 assumes that two marked subunit are sufficient to alter the phenotype of the receptor.

(C) Pattern of phenotype expression predicted by the various models, following cotransfection of wild-type 2_Q with marked 2_R. The fraction of receptors expressing the marker phenotype is plotted against the fraction of marked subunits.

(D) Pattern of phenotype expression following cotransfection of 2_Q with marked 2_Q.

(E) Pattern of phenotype expression following cotransfection of 2_R with marked 2_Q.

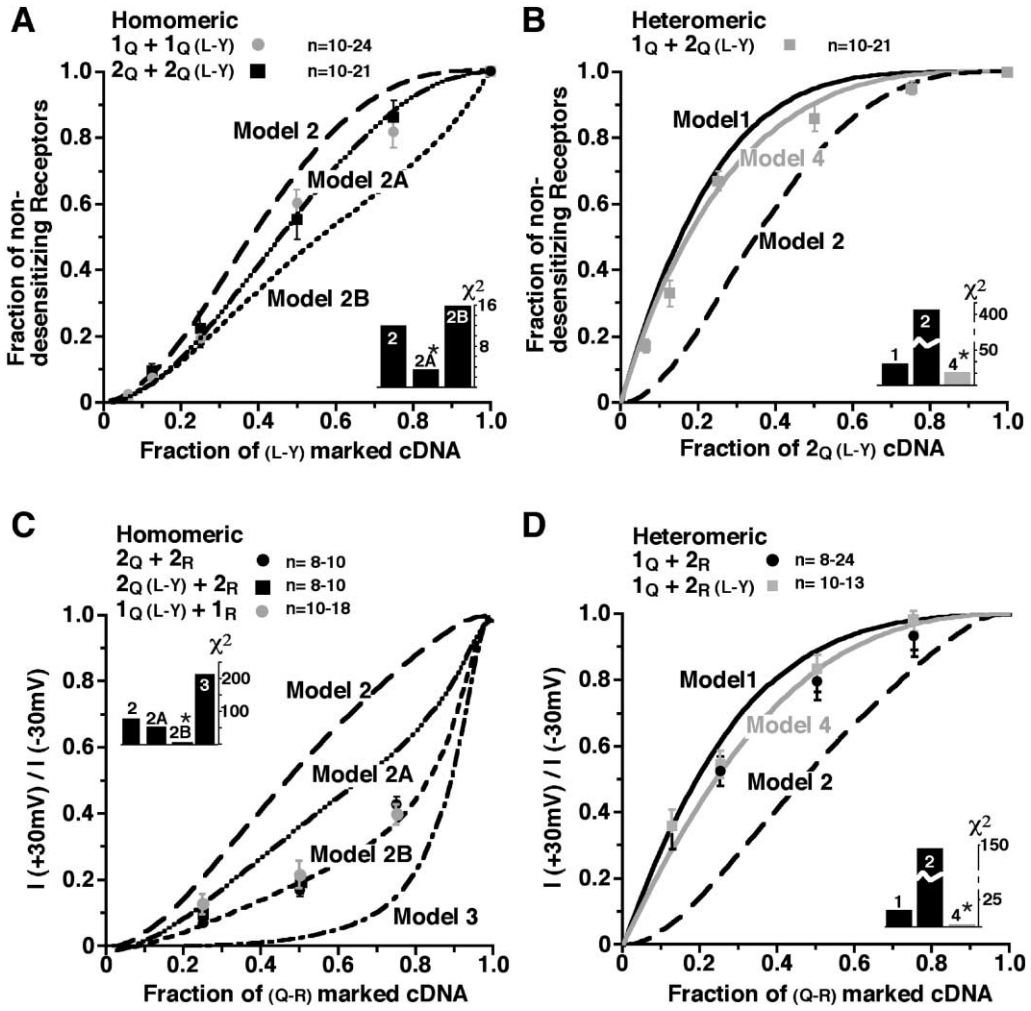

Figure 3. Binomial Assembly of Homomeric Receptors and Selective Assembly of Heteromeric Receptors

(A) Summary of results from homomeric $1_Q + 1_Q$(L-Y) and $2_Q + 2_Q$(L-Y) cotransfection experiments. The nondesensitization index is plotted against the fraction of DNA carrying the nondesensitizing L-Y marker. The data were compared to the predictions of Models 2, 2A, and 2B (dashed lines). Goodness of fit was assessed for $2_Q + 2_Q$(L-Y) using the χ^2 statistic (inset). n is the number of outside-out patches.

(B) Summary of results from heteromeric $1_Q + 2_Q$(L-Y) cotransfection experiments. The results are compared to the predictions of Models 1, 2, and 4.

(C) Summary of homomeric $2_Q + 2_R$, 2_Q(L-Y)$+ 2_R$ and 1_Q(L-Y)$+ 1_R$ cotransfection experiments. The nonrectification index is plotted against the fraction of cDNA carrying the nonrectifying Q-R marker, and compared to the predictions of Models 2, 2A, 2B, and 3.

(D) Summary of heteromeric $1_Q + 2_R$ and $1_Q + 2_R$(L-Y) cotransfection experiments. The results are compared to the predictions of Models 1, 2, and 4.

data, and the reproducibility within and between many independent data sets (Figures 3 and 4), provide further confirmation that the assumptions are reasonable and the parameter estimates are accurate.

Selective Assembly of Heteromeric AMPA Receptors

The predictions of the phenotype expression models were compared with the expression data obtained with many different subunit combinations (Figures 3 and 4). Several clear and reproducible results emerged. As expected, the homomeric data (lefthand panels) were accurately described by a random assembly model in every case. The phenotype expression data for the nondesensitization marker was best described by Model 2A (Figure 3A), and for the nonrectification marker by Model 2B (Figure 3C). In contrast, the heteromeric data (right hand panels) were not adequately described by any of the random assembly models. The selective assembly Model 4 provides a better description of heteromeric phenotype expression for both the Q→R and L→Y markers (Figures 3B and 3D). The nondesensitization marker results were confirmed using additional subunit combinations. In every case, the phenotype expression data for homomeric receptors was best described by a random assembly model (Figures 4A and 4C) and for heteromeric receptors by a selective assembly model (Figures 4B and 4D). We can therefore reject the hypothesis that heteromeric receptors assemble randomly (Figure 1F, Model 1). Taken together, the data show that heteromeric subunits selectively assemble into a config-

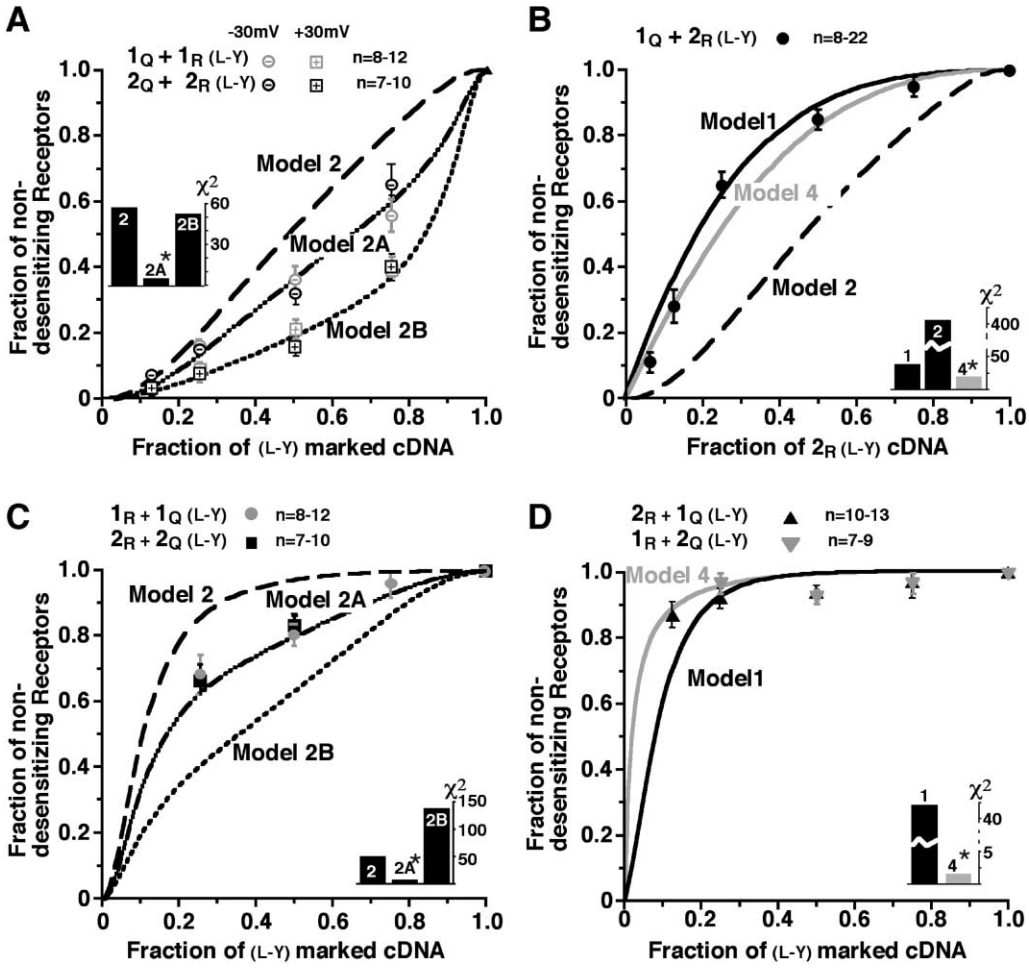

Figure 4. More Evidence Concerning Receptor Assembly

(A) Summary of results from homomeric $1_Q + 1_R$(L-Y) and $2_Q + 2_R$(L-Y) cotransfection experiments. The nondesensitization index is plotted against the fraction of cDNA carrying the L-Y marker. Experiments were performed at −30 mV and +30 mV. At positive membrane potentials, the fraction of nondesensitizing receptors was calculated as steady-state current at +30 mV/steady-state current at −30 mV in the presence of cyclothiazide. The data were compared to the predictions of Models 2, 2A, and 2B (dashed lines). Goodness of fit was assessed for results obtained at −30 mV using the χ^2 statistic (inset).

(B) Summary of results from heteromeric $1_Q + 2_R$(L-Y) cotransfection experiments. The nondesensitization index is plotted against the fraction of 2_R(L-Y) cDNA, and compared to the predictions of Models 1, 2, and 4.

(C) Summary of results from homomeric $1_R + 1_Q$(L-Y) and $2_R + 2_Q$(L-Y) cotransfection experiments. The nondesensitization index is plotted against the fraction of cDNA carrying the L-Y marker, and compared to the predictions of Models 2, 2A, and 2B.

(D) Summary of results from heteromeric $2_R + 1_Q$(L-Y) and $1_R + 2_Q$(L-Y) cotransfection experiments. The results are compared to the predictions of Models 1 and 4.

uration that expresses both the L→Y and Q→R phenotypes (Figure 1G, Model 4).

Model 4 arbitrarily assumes that a symmetric configuration is favored. To determine the actual subunit configuration of heteromeric AMPA receptors, we need to understand how the spatial arrangement of marked subunits is related to channel phenotype.

Spatial Arrangement of Subunits Controls Channel Properties

Analyzing the phenotype expression pattern of homomeric subunits is relatively straightforward because we can be confident that they assemble randomly. We coexpressed homomeric $2_Q + 2_Q$(L-Y) and plotted the nondesensitization index as a function of marked DNA fraction (Figure 3A). Essentially, identical results were obtained with $1_Q + 1_Q$(L-Y) cotransfection (Figure 3A) (but see Thalhammer et al., 1999). All channels have the same conductance for these two subunit combinations, which simplifies the assumptions underlying the phenotype expression models. The data were best described by Model 2A (Figure 3A), which implies that channels with two marked subunits on opposite sides of the channel pore (symmetric heterodimers) are desensitizing, but channels with marked subunits positioned side by side (polar heterodimers) are nondesensitizing. Thus, both the stoichiometry and spatial arrangement of the subunits influence channel properties. The goodness-of-fit for the various models was assessed using the χ^2 statistic (see insert). The data were accurately described by

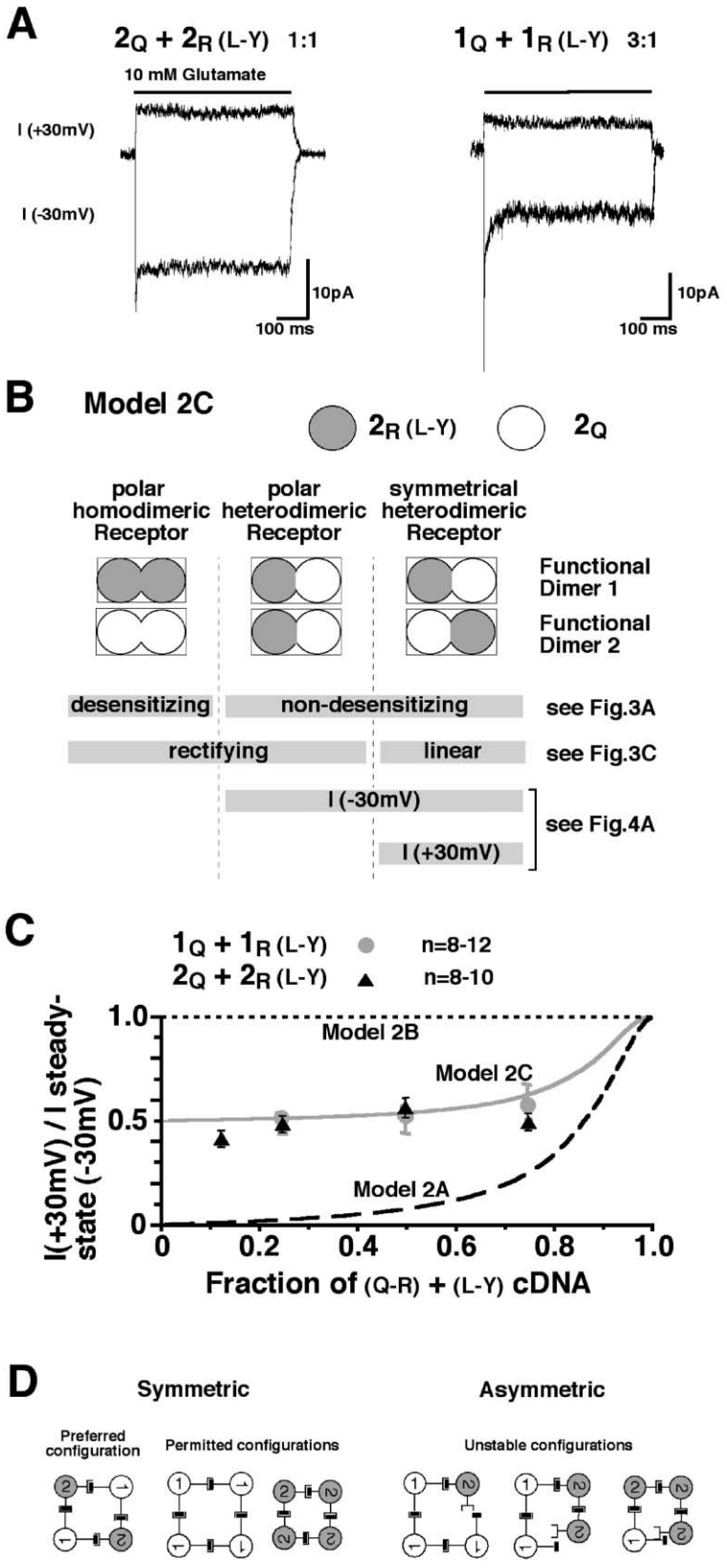

Figure 5. Receptors Assemble as a Dimer of Dimers

(A) Typical responses from a patch containing $2_Q + 2_R$(L-Y) at a ratio of 1:1 (left), and from a patch containing $1_Q + 1_R$(L-Y) at a ratio of 3:1 (right), recorded at −30 mV and at +30 mV. Models 2A and 2B predict that both responses should desensitize strongly at +30 mV, but no desensitization was seen.

(B) Model 2C predicts the distribution of marker phenotypes for 2:2 heteromers, based on the assumption that AMPA receptors assemble and function as a pair of dimers. Desensitization and rectification properties are shown for receptors assembled from 2_Q (white circles) and 2_R(L-Y) (gray circles). The pairs of fused circles represent functional dimers within the assembled receptor.

(C) The ratio of nondesensitizing outward current versus inward steady-state current for $1_Q + 1_R$(L-Y) and $2_Q + 2_R$(L-Y) cotransfections. The phenotype expression patterns predicted by Models 2A, 2B, and 2C are superimposed.

(D) Symmetry-controlled assembly model. Schematic representation of how simple geometric factors such as different intersubunit bond lengths for GluR1 and GluR2 favors symmetric subunit assemblies, and may destabilize asymmetric subunit arrangements due to misalignment of subunit-subunit interfaces, or steric hindrance.

Model 2A, while all other models could be rejected ($p < 0.05$). As an independent test, we coexpressed $1_Q + 1_R$(L-Y) and $2_Q + 2_R$(L-Y). The predictions of the phenotype expression models are more widely separated because of the relatively low conductance of 1_R and 2_R homomers. Again, the data were accurately described

by Model 2A, while all other models could be rejected ($p < 0.05$, Figure 4A).

We next tested whether nonrectification followed a similar pattern of phenotype dominance. We coexpressed $2_Q + 2_R$ and plotted the nonrectification index as a function of marked subunit fraction (Figure 3C). Essentially identical results were obtained when their nondesensitizing analogs on either GluR1 or GluR2 subunits were coexpressed. The results strongly favor Model 2B, which implies that channels with two marked subunits arranged side by side are rectifying, but channels with two marked subunits located on opposite sides of the channel pore conduct linearly. The goodness-of-fit for the various models was assessed using the χ^2 statistic. The data were accurately described by Model 2B, while all other models could be rejected ($p < 0.05$, Figure 3C insert). Again, the spatial arrangement of the subunits determines the channel properties.

AMPA Receptors Assemble as a Pair of Dimers

We used a subunit carrying both markers to crosscheck the above results. 1_Q was coexpressed with 1_R(L-Y) and 2_Q was coexpressed with 2_R(L-Y) and the desensitization indices were plotted as a function of marked subunit fraction at both −30 mV and at +30 mV (Figure 4A). Given the above results, symmetric heterodimers should desensitize (desensitization index follows Model 2A) and should be nonrectifying (nonrectification index follows Model 2B). Consequently, the response at +30 mV should desensitize strongly resulting in a very small steady-state current. In fact, the steady-state response was large (about 50% of the response at −30 mV) and did not exhibit any desensitization (Figure 5A). To explain this unexpected result, we had to abandon Model 2B and develop another phenotype expression model. We assumed that AMPA receptors are structured as a pair of dimers, and nondesensitizing receptors must have at least one L→Y marker in both dimers (Model 2C, Figure 5B). This model is based on the idea that desensitization is only blocked when a mutant tyrosine residue is present at the dimer interface in both dimers. Model 2C predicts that symmetric heterodimers will not desensitize, and the steady-state current at positive potentials will be approximately half the steady-state current at negative potentials, consistent with the data (Figure 5A). The ratio of steady-state current at positive and negative potentials was plotted against the fraction of L→Y mutant cDNA, and the results were compared with the model predictions (Figure 5C). The results strongly favor Model 2C, and support the hypothesis that AMPA receptor subunits are assembled as a pair of dimers (Armstrong and Gouaux, 2000).

To crosscheck these findings, we also tested a cotransfection of 2_R with 2_Q(L-Y). At a 1:1 DNA ratio, the outward current at +30 mV did not desensitize, and was not potentiated by 100 μM cyclothiazide (0.98 ± 0.02, n = 12), consistent with Model 2C, but not Model 2A (results not shown). Thus, 1:3 heteromers and 2_R homomers, which should be nonrectifying and desensitizing, must have very low conductances. This result provides support for the conductance parameters used in the phenotype expression models. In addition, the steady-state amplitude of the response at −30 mV was weakly potentiated by cyclothiazide (13% ± 3%, n = 12). Model 2C predicts cyclothiazide potentiation of 20%, similar to the observed potentiation. This finding is consistent with the idea that polar homodimeric receptors desensitize (Figure 5B), and would therefore be potentiated by cyclothiazide.

In summary, our data suggest that AMPA receptors are structured as a pair of dimers, and that both the stoichiometry and the spatial organization of marked subunits within a channel determines its phenotype. This information can now be used to determine the preferred subunit configuration of heteromeric AMPA receptors.

Heteromeric AMPA Receptors Preferentially Assemble as Symmetric Heterodimers

We have shown that heteromeric AMPA receptors assemble with a preferred subunit configuration. When the GluR2 subunit carries a nondesensitizing or a nonrectifying marker, the preferred configuration expresses the marker phenotype (Figures 3B and 3D). If we assume that the same rules of phenotype expression apply to homomeric and heteromeric receptors, then we can determine the preferred subunit configuration. The only two configurations that express both marker phenotypes are symmetric heterodimers (Figure 5B), and 1:3 heteromers. However, we have also shown that 1:3 heteromers carrying the Q-R marker must have a very low conductance (Figure 5C), so this option can be ruled out. Thus, by process of elimination, heteromeric AMPA receptor subunits must preferentially assemble in a symmetric heterodimer configuration.

Discussion

In this study, we have investigated how the subunit composition of AMPA receptors influences channel gating. By utilizing two independent marker mutations, we obtained surprisingly detailed insights into receptor structure and function. The first major finding was that the spatial arrangement of subunits determines the desensitization and rectification properties of the receptor/channel. For homomeric receptors, interactions within the dimerized extracellular domain control the desensitization process, while linear conductance requires two arginine-containing subunits positioned on opposite sides of the channel pore. The information derived from homomeric receptors was used to investigate the assembly of heteromeric subunits. The second major finding was that for GluR1/GluR2 heteromers, the distribution of subunit assemblies was not random, but strongly favored a stoichiometry of two GluR1 and two GluR2 subunits in a symmetric arrangement.

Heteromeric Receptor Assembly Mechanism

The phenotype expression model for heteromeric AMPA receptors, Model 4, provides no insight into the physical mechanisms that might produce selective assembly. We propose two hypothetical mechanisms that could explain the selective assembly of symmetric heterodimers. The first hypothesis is that steric hindrance or interface mismatch in the tetrameric receptor structure may destabilize asymmetric subunit assemblies. Destabiliza-

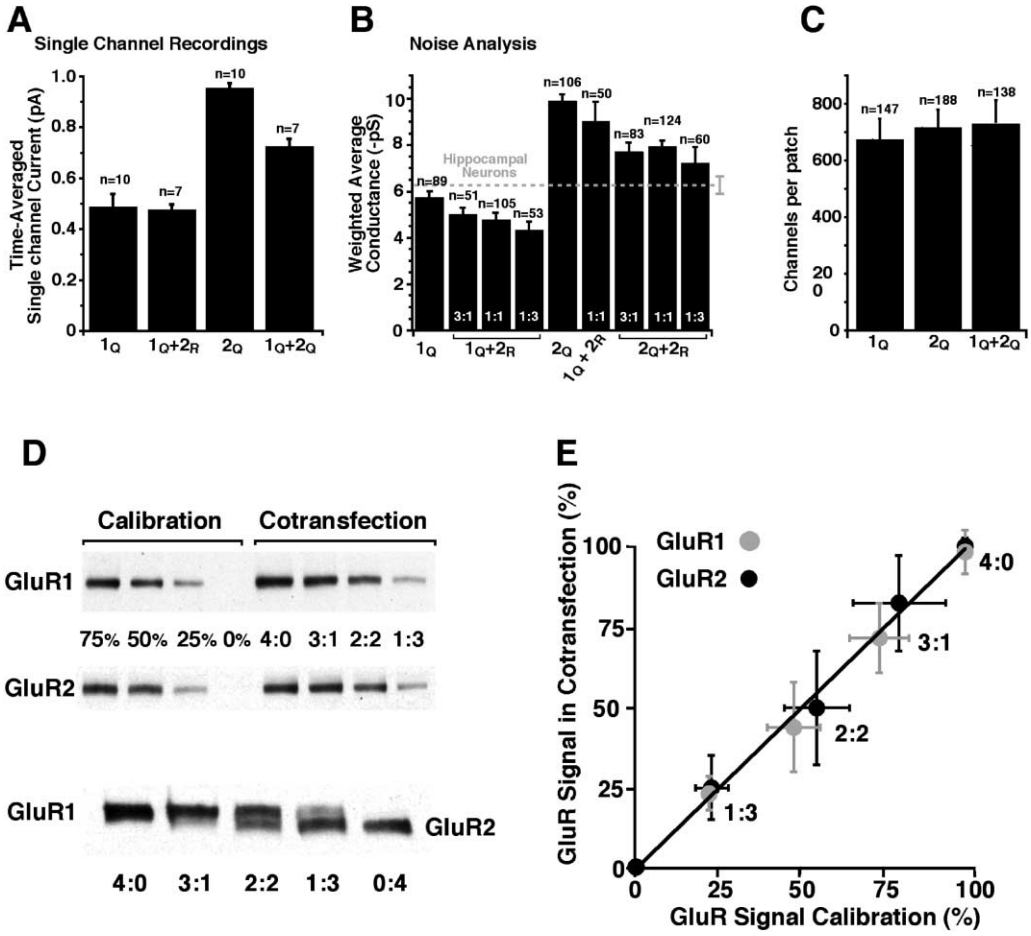

Figure 6. Validation of Model Assumptions

(A) Summary results from single channel experiments. Patches containing a single channel were pulled from HEK cells transfected with 1_Q, or with 2_Q, or cotransfected with $1_Q + 2_Q$ or $1_Q + 2_R$ at a ratio of 1:1. The bar plot shows the time-averaged single channel current for each subunit combination. n is the number of patches analyzed.

(B) Summary results from multichannel experiments. Weighted average single channel conductance estimated by noise analysis for various subunit combinations. Experiments were performed on 10–24 patches for each subunit combination. n is the number of traces used for fluctuation analysis. The single channel conductance of native AMPA channels from hippocampal neurons is indicated by a dotted line.

(C) The average number of channels per outside-out membrane patch for cells transfected with 1_Q, or with 2_Q or cotransfected with $1_Q + 2_Q$ (1:1 ratio), calculated from the current in the presence of 100 μM cyclothiazide divided by the average single channel current. The same total amount of cDNA was used in all transfections.

(D) Relative protein expression correlates with the amount of transfected plasmids. Plasmids encoding either for GluR1 or for GluR2 subunits (4:0 or 0:4), or mixed together in different ratios (3:1, 2:2, 1:3), were transfected into HEK293 cells. For calibration, various dilutions of 1Q or 2R subunit protein (75%, 50%, and 25%) were loaded on a 6% SDS gel together with undiluted protein from the cotransfections. Blotted proteins were detected by specific polyclonal antibodies. The lower panel shows the relative expression of both cotransfected subunits revealed by incubating a blot with both specific antibodies. Where paired bands are visible, the upper band corresponds to GluR1 and the lower band to GluR2.

(E) Signals from the GluR1- and GluR2-specific lanes were densitometrically quantified. Signals from cotransfected GluR1 (white circles) and GluR2 (gray circles) are plotted against the corresponding calibration signals (three independent cotransfections). Signals were normalized to the undiluted homomeric transfection. Two undiluted lanes were run to asses systematic errors in the densiometric analysis. GluR subunit expression varied linearly with cDNA concentration.

tion could arise from simple geometric factors such as different intersubunit bond lengths, as shown schematically for symmetric and asymmetric assemblies (symmetry-controlled assembly, Figure 5D). If it is further assumed that subunit-subunit binding is reversible, and that all expressed subunits eventually equilibrate into one of the three stable symmetric configurations, then this mechanism leads to a binomial distribution similar to Model 4 (Figure 2B). Another hypothetical assembly mechanism assumes that receptor formation results from the consecutive association of monomers to form a tetramer, and that GluR2 dimerizes with GluR1 more rapidly than other subunit pairings. This might occur if the physical profile of the righthand interface of GluR2 closely matched the profile of the lefthand interface of GluR1 (association-controlled assembly). A chemical-kinetic model of the assembly process was constructed, based on this mechanism. The phenotype expression data for several different subunit combinations were best fit when GluR2 binds to GluR1 five times faster

than other subunit combinations (results not shown). This mechanism also strongly favors the assembly of symmetric heterodimers.

The actual assembly mechanism may be some combination of these two hypothetical mechanisms, or it may involve interactions with other proteins. None the less, it is clear that coexpressed GluR1/GluR2 preferentially assemble as symmetric heterodimers. The result is a highly homogenous receptor population.

Functional Implications

From an evolutionary viewpoint, it is attractive for cells to perform basic biological functions using modular protein structures built by combining several different subunits. Modular construction can produce multimers with diverse and flexible properties controlled by gene expression levels. It is well known that the pattern of expression of receptor subunits can change during development, altering the kinetics, pharmacology, and other properties of the assembled receptor (Dingledine et al., 1999). It is likely that the spatial arrangement of the subunits is important for optimal function. Evolution may therefore have provided a mechanism that promotes the assembly of subunits in their optimal configuration. Symmetry-controlled assembly and association-controlled assembly are two candidate mechanisms, and both have the practical advantage of being built in to the protein subunits themselves. There is no need for an external mechanism, such as a catalytic enzyme.

Recent data on dimerization in homomers using a biochemical assay for GluR4 homomeric receptor assembly (Kuusinen et al., 1999), and the crystallization of the extracellular ligand binding core of GluR2 subunits (Armstrong and Gouaux, 2000), provide a basis for speculating that dimerization promotes the consistent assembly of AMPA receptors in an optimal configuration. Indeed, dimerization may be a general principle guiding the assembly of multimeric channels, as a similar mechanism has been proposed for K^+-channels (Tu and Deutsch, 1999) and for cyclic nucleotide-gated channels (Liu et al., 1998). Our results support the suggestion that interactions between residues at the dimer interface influence the desensitization process (Figure 5). This does not rule out the possibility that other subunit interactions (for example, at the transmembrane region or the N terminus preceding the S1 binding region) are important for preferential assembly of symmetric heterodimers (Ayalon and Stern-Bach, 2001). In summary, we propose that symmetry-controlled or association-controlled assembly of heteromeric AMPA receptors has evolved to reduce structural and functional heterogeneity in the receptor population. Similar mechanisms are likely to control the assembly of other functional multimers.

Experimental Procedures

Phenotype Expression Models

The phenotype expression models incorporate estimates of the average steady-state current contributed by each AMPA channel configuration. Only the relative conductance values for the various configurations were needed for the model, and they were estimated as follows. Patches containing a single channel were obtained as previously described (Rosenmund et al., 1998). Recordings where made at −80 mV in the presence of a saturating concentration of agonist and cyclothiazide, and the average steady-state current was measured directly (this current is equal to the single channel current multiplied by open probability, summed over all subconductance states). A few patches contained 2 or 3 channels, but open probability was high (>0.5) so the number of channels could be reliably determined from the maximum observed current divided by the dominant single channel current (Yamada and Tang, 1993; Rosenmund et al., 1998; Smith et al., 2000). The average steady-state current for the patch was divided by the number of channels present. We tested homomeric 1_Q and 2_Q channels, and heteromeric channels produced by cotransfection of $1_Q + 2_{Q/R}$ at a ratio of 1:1 (Figure 6A). The single channel results for heteromeric cotransfection are dominated by channels with the preferred heteromeric subunit configuration. In contrast, homomeric cotransfections produce many different subunit combinations. A much larger number of single channel recordings would be needed to adequately sample this mixed population, and the results would be difficult to interpret. Instead, we recorded from patches containing many channels and applied steady-state mean-variance noise analysis, which estimates the weighted average single channel conductance for a mixed population of receptors (Traynelis et al., 1993; Neher and Stevens, 1977). Noise analysis requires that the channel open probability is <30%, so cyclothiazide was not added. This technique permitted us to efficiently analyze a range of subunit combinations (Figure 6B). Note that the pattern of average conductances for 1_Q and 2_Q homomers, and $1_Q + 2_{Q/R}$ heteromers (Figure 6B), closely parallels the pattern of average single channel currents (Figure 6A), which confirms the utility of the noise analysis approach. Cotransfection experiments of 1_Q with 2_R yielded conductance levels of about 5 pS, similar to results from hippocampal neurons (6.3 ± 0.4 pS, n = 26, Figure 6B). The single channel conductivity did not decrease significantly with increasing amounts of 2_R, consistent with the assumption that assemblies containing three 2_R subunits have low conductance, similar to 2_R homomers (Swanson et al., 1997).

These experimental results were used as a guide when selecting single channel current parameters for the phenotype expression models (see Results). We are confident that these parameter estimates are reasonably accurate. Independent support is provided by the excellent agreement between the predictions of binomial assembly models and homomeric coexpression data obtained with many different subunit combinations. For example, Model 2A accurately predicts the nondesensitization data for $2_Q + 2_Q$(L-Y) and for $2_Q + 2_R$(L-Y) at −30 mV. If there was a serious error in the single channel current parameters for Q/R assemblies, then these internally consistent results would not be expected, and the phenotype expression data would deviate from binomial predictions.

Channel Expression Correlates with the Transfected DNA Concentration

The assembly models assume that the ratio of marked and unmarked DNA is maintained through the transcription, translation, and transport processes that lead to receptor expression at the cell surface. We used vectors for the GluR coexpression that differed only in the insert coding the receptor subunit. For most of the experiments, the inserts only differed at a single amino acid residue, and were unlikely to yield different expression levels. A previous study found no significant difference in the efficiency of cell surface expression for GluR1 and GluR2 subunits (Hall et al., 1997).

We assessed the level of functional expression by quantifying the number of ion channels in outside-out patch experiments. HEK cells were transfected with 1_Q or 2_Q, and the same total quantity of DNA was used in the transfections. The number of channels in a patch was estimated from the total steady-state current divided by the steady-state current for a single channel. The average number of channels per patch was independent of the expressed subunits (Figure 6C). Thus, the functional expression of channels is correlated with the amount of DNA used in the transfection.

To determine whether protein expression was linearly correlated with the amount of cDNA used in a transfection, we cotransfected GluR1 and GluR2 subunits and estimated their relative expression levels using biochemical techniques. HEK cells were transfected with $GluR1_R$ and $GluR2_Q$ at ratios of 4:0, 1:3, 2:2, 3:1, and 0:4, main-

taining a constant total DNA concentration. Cells were harvested and GluR expression examined in Western blots using GluR1- and GluR2-specific antibodies (Figure 6D). Densitometric analysis revealed that subunit expression correlated well with the amount of DNA used in the transfection (Figure 6E). This method does not distinguish between GluR subunits located at the surface membrane and those located within intracellular compartments. However, the detection of an approximately constant number of channels from patch to patch, independent of GluR subunit type (Figure 6C), argues that all types of GluR subunits used in this study are efficiently incorporated into the cell membrane. Thus, the number of GluR subunits that are available for assembly into functional channels most likely varies as a linear function of DNA concentration.

The reproducible nature of the results obtained with different subunit combinations also suggests that we have good control over the level of subunit expression. For example, the phenotype expression patterns of homomeric $1_Q + 1_R$(L-Y), $2_Q + 2_R$, $2_Q + 2_R$(L-Y), and 2_Q(L-Y) + 2_R(L-Y) are indistinguishable, and the error bars on individual data points are small (Figure 1C). Similarly, the expression patterns of heteromeric $1_Q + 2_R$, and 1_Q(L-Y) + 2_R and 2_Q(L-Y) + 1_R are indistinguishable (Figure 1D). These results support the assumption that functional subunit expression is highly correlated with the amount of transfected DNA.

Plasmids and Mutagenesis

cDNAs encoded the alternatively spliced flip version of wild-type $GluR1_Q$ and $GluR2_{Q/R}$ (Sommer et al., 1990). Point mutations were introduced using the PCR-based method described by the "QuickChange" mutagenesis manual (Stratagene). An L→Y point mutation was introduced at position L497 in the GluR1 subunit, and at the corresponding position L504 in the GluR2 subunit. Mutations were verified by double-strand DNA sequencing. All receptors were subcloned into pRK5 vectors (InVitrogen). Amino acid numbering starts from the first methionine of the open reading frame.

Cell Culture and Cotransfections

Human embryonic kidney cell line HEK293 (ATCC, USA) was cultured in RPMI 1640 (Gibco BRL) supplemented with 10% fetal calf serum. Cells were passaged up to 15 times. For $Ca_2(PO_4)_3$-based transfections (Chen and Okayama, 1988), cells were plated at a density of 2×10^5 per 35 mm dish using a total concentration of 3 μg cDNA encoding the wild and mutant AMPA receptors. Transfected cells were detected by cotransfecting with the plasmid encoding cDNA for green fluorescent protein. Cells were washed with RPMI 1640 medium 6–8 hr after transfection, and were used for electrophysiological recordings after 24 hr. Neurons were cultured as previously described (Bekkers and Stevens, 1991) and were used for recordings 1–2 weeks after plating.

For quantitative Western blot analysis of glutamate receptor expression, HEK293 cells were transiently transfected with plasmids coding for $GluR1_Q$ and $GluR2_R$ either alone or at indicated ratios by LipofectAMINE (Life Technologies, Gaithersburg, MD). After 60 hr, cells were washed briefly with PBS, harvested, and homogenized in ice-cold lysis buffer (50 mM Tris/HCl, pH 7.4, 150 mM NaCl, 1% NP-40, 0.5% Deoxycholate, protease inhibitors [1 μg/ml leupeptin, 1 μg/ml pepstatin A, 2 μg/ml aprotenin, and 1 mM PMSF]). Nonsoluble components were removed by centrifugation at 4°C and protein concentration was determined. Equal amounts of proteins were used for SDS-PAGE and blotted onto nitrocellulose membrane. The recombinant-expressed glutamate receptors were probed with polyclonal rabbit Anti-Glutamate Receptor 1 (1:5000, Chemicon, Temecula, CA) and polyclonal rabbit Anti-Glutamate Receptor 2/3 (1:3000, Calbiochem, Cambridge, MA). Blots were developed using horseradish peroxidase-conjugated AffiniPure goat Anti-Rabbit IgG (1:10000, Jackson ImmunoResearch Laboratories, West Grove, PA) together with the ECL™ Western blotting detection reagent (Amersham Pharmacia Biotech, Piscataway, NJ), and chemoluminescence was documented on Hyperfilm™ ECL™. Quantification of protein expression including calibration was determined using the "Densitometric Analysis of 1-D Gels" macro from the image analysis program NIH Image 1.62. Calibration was performed by loading relative amounts (75%, 50%, 25%) of homomeric expressed GluR1 and GluR2, and signals were plotted on the *x* axis against the signals from the cotransfections performed in parallel (4:0, 3:1, 2:2, 1:3, Figure 6E). Signals were background subtracted.

Electrophysiology

Outside-out membrane patches were excised from HEK293 cell expressing wild-type and mutant receptors, and from primary cultured mouse hippocampal neurons. Patches were positioned in front of a fast perfusion system consisting of a theta tube flow pipe mounted on a piezoelectric translator (Clements and Westbrook, 1991; Colquhoun et al., 1992). At the completion of a recording, solution exchange time (20%–80% to peak) was estimated from open tip control and ranged from 0.3–0.6 ms. Experiments were performed at room temperature. Agonist application was repeated at 0.2–0.02 Hz. Patch pipettes had a resistance of 2–4 MΩ, and were filled with a solution containing 150 mM CsF, 20 mM HEPES, 10 mM NaCl, 10 mM EGTA, adjusted to 355 mOsm (pH 7.3), to which 50 μM spermine was added. The extracellular medium contained 170 mM NaCl, 10 mM HEPES, 10 mM glucose, 4 mM $CaCl_2$, 4 mM $MgCl_2$, adjusted to 355 mOsm (pH 7.25). For experiments on neuronal patches, TTX was added. Agonist solutions were made by mixing external medium with isotonic agonist stock solutions (355 mOsm, pH 7.25). Cyclothiazide was dissolved in DMSO before dilution with extracellular solution. Holding potential was typically −60 mV. Currents were filtered at 2 kHz and digitized at 20 kHz.

Data Analysis

Analysis was performed using AxoGraph 4 software (Axon Instr.) and graphed using KaleidaGraph 3.5 (Synergy Software). Homomeric glutamine-containing GluR1 or GluR2 receptors did not rectify completely, but produced an outward current at +30 mV that was 9% of the inward current at −30 mV. This outward current and the exact reversal potential were used in the estimation of the linear and rectifying receptor populations. When desensitizing and nondesensitizing receptors were cotransfected, the total receptor population was determined by the coapplication of glutamate and 100 μM cyclothiazide. At this concentration, cyclothiazide causes a mild block of inward current (≈ 11%), which has previously been observed in wild-type (Partin et al., 1995) and nondesensitizing receptors mutants (Stern-Bach et al., 1998). This block was incorporated into the estimation of total receptor population. The steady-state component of the desensitizing response was subtracted before estimating the nondesensitizing receptor population.

Data are presented as mean ± SEM, and "n" is the number of outside-out patches, unless otherwise indicated.

Acknowledgments

We thank Dr. Yael Stern-Bach for providing the point mutant receptors used in this study and for comments on the manuscript, Dr. Peter Seeburg for providing the pRK5 wild-type GluR1/GluR2 receptors, Ina Herfort for assistance with cell culture, Dr. Erwin Neher for critically reviewing this manuscript, Dr. Volker Scheuss for initial help with modeling, Dirk Reuter for help with amplifying cDNA, and Sebastian Russo for participation in preliminary experiments. This work was supported by the Max-Planck Society, and by a Grant from the G.I.F., the "German-Israeli Foundation for Scientific Research and Development."

Received March 7, 2001; revised October 3, 2001.

References

Armstrong, N., and Gouaux, E. (2000). Mechanisms for activation and antagonism of an AMPA-sensitive glutamate receptor: crystal structures of the GluR2 ligand binding core. Neuron *28*, 165–181.

Ayalon, G., and Stern-Bach, Y. (2001). Functional assembly of AMPA and kainate receptors is mediated by several discrete protein-protein interactions. Neuron *31*, 103–113.

Bekkers, J.M., and Stevens, C.F. (1991). Excitatory and inhibitory autaptic currents in isolated hippocampal neurons maintained in cell culture. Proc. Natl. Acad. Sci. USA *88*, 7834–7838.

Bowie, D., and Mayer, M.L. (1995). Inward rectification of both AMPA

and kainate subtype glutamate receptors generated by polyamine-mediated ion channel block. Neuron *15*, 453–462.

Burnashev, N., Monyer, H., Seeburg, P.H., and Sakmann, B. (1992). Divalent ion permeability of AMPA receptor channels is dominated by the edited form of a single subunit. Neuron *8*, 189–198.

Chen, C.A., and Okayama, H. (1988). Calcium phosphate-mediated gene transfer: a highly efficient transfection system for stably transforming cells with plasmid DNA. Biotechniques *6*, 632–638.

Clements, J.D., and Westbrook, G.L. (1991). Activation kinetics reveal the number of glutamate and glycine binding sites on the N-methyl-D-aspartate receptor. Neuron *7*, 605–613.

Colquhoun, D., Jonas, P., and Sakmann, B. (1992). Action of brief pulses of glutamate on AMPA/kainate receptors in patches from different neurones of rat hippocampal slices. J. Physiol. *458*, 261–287.

Dingledine, R., Borges, K., Bowie, D., and Traynelis, S.F. (1999). The glutamate receptor ion channels. Pharmacol. Rev. *51*, 7–61.

Donevan, S.D., and Rogawski, M.A. (1995). Intracellular polyamines mediate inward rectification of Ca(2+)-permeable alpha-amino-3-hydroxy-5-methyl-4-isoxazolepropionic acid receptors. Proc. Natl. Acad. Sci. USA *92*, 9298–9302.

Geiger, J.R., Melcher, T., Koh, D.S., Sakmann, B., Seeburg, P.H., Jonas, P., and Monyer, H. (1995). Relative abundance of subunit mRNAs determines gating and Ca2+ permeability of AMPA receptors in principal neurons and interneurons in rat CNS. Neuron *15*, 193–204.

Hall, R.A., Hansen, A., Andersen, P.H., and Soderling, T.R. (1997). Surface expression of the AMPA receptor subunits GluR1, GluR2, and GluR4 in stably transfected baby hamster kidney cells. J. Neurochem. *68*, 625–630.

Hume, R.I., Dingledine, R., and Heinemann, S.F. (1991). Identification of a site in glutamate receptor subunits that controls calcium permeability. Science *253*, 1028–1031.

Iino, M., Mochizuki, S., and Ozawa, S. (1994). Relationship between calcium permeability and rectification properties of AMPA receptors in cultured rat hippocampal neurons. Neurosci. Lett. *173*, 14–16.

Jonas, P., and Burnashev, N. (1995). Molecular mechanisms controlling calcium entry through AMPA-type glutamate receptor channels. Neuron *15*, 987–990.

Jonas, P., Racca, C., Sakmann, B., Seeburg, P.H., and Monyer, H. (1994). Differences in Ca2+ permeability of AMPA-type glutamate receptor channels in neocortical neurons caused by differential GluR-B subunit expression. Neuron *12*, 1281–1289.

Kamboj, S.K., Swanson, G.T., and Cull-Candy, S.G. (1995). Intracellular spermine confers rectification on rat calcium-permeable AMPA and kainate receptors. J. Physiol. *486*, 297–303.

Koh, D.S., Burnashev, N., and Jonas, P. (1995). Block of native Ca(2+)-permeable AMPA receptors in rat brain by intracellular polyamines generates double rectification. J. Physiol. *486*, 305–312.

Kuusinen, A., Abele, R., Madden, D.R., and Keinanen, K. (1999). Oligomerization and ligand-binding properties of the ectodomain of the alpha-amino-3-hydroxy-5-methyl-4-isoxazole propionic acid receptor subunit GluRD. J. Biol. Chem. *274*, 28937–28943.

Liu, D.T., Tibbs, G.R., Paoletti, P., and Siegelbaum, S.A. (1998). Constraining ligand-binding site stoichiometry suggests that a cyclic nucleotide-gated channel is composed of two functional dimers. Neuron *21*, 235–248.

Mano, I., and Teichberg, V.I. (1998). A tetrameric subunit stoichiometry for a glutamate receptor-channel complex. Neuroreport *9*, 327–331.

Neher, E., and Stevens, C.F. (1977). Conductance fluctuations and ionic pores in membranes. Annu. Rev. Biophys. Bioeng. *6*, 345–381.

Partin, K.M., Bowie, D., and Mayer, M.L. (1995). Structural determinants of allosteric regulation in alternatively spliced AMPA receptors. Neuron *14*, 833–843.

Raman, I.M., Zhang, S., and Trussell, L.O. (1994). Pathway-specific variants of AMPA receptors and their contribution to neuronal signaling. J. Neurosci. *14*, 4998–5010.

Robert, A., Irizarry, S.N., Hughes, T.E., and Howe, J.R. (2001). Subunit interactions and AMPA receptor desensitization. J. Neurosci. *21*, 5574–5586.

Rosenmund, C., Stern-Bach, Y., and Stevens, C.F. (1998). The tetrameric structure of a glutamate receptor channel. Science *280*, 1596–1599.

Seeburg, P.H., Higuchi, M., and Sprengel, R. (1998). RNA editing of brain glutamate receptor channels: mechanism and physiology. Brain Res. Brain Res. Rev. *26*, 217–229.

Smith, T.C., Wang, L.Y., and Howe, J.R. (2000). Heterogeneous conductance levels of native AMPA receptors. J. Neurosci. *20*, 2073–2085.

Sommer, B., Keinanen, K., Verdoorn, T.A., Wisden, W., Burnashev, N., Herb, A., Kohler, M., Takagi, T., Sakmann, B., and Seeburg, P.H. (1990). Flip and flop: a cell-specific functional switch in glutamate-operated channels of the CNS. Science *249*, 1580–1585.

Stern-Bach, Y., Russo, S., Neuman, M., and Rosenmund, C. (1998). A point mutation in the glutamate binding site blocks desensitization of AMPA receptors. Neuron *21*, 907–918.

Swanson, G.T., Kamboj, S.K., and Cull-Candy, S.G. (1997). Single-channel properties of recombinant AMPA receptors depend on RNA editing, splice variation, and subunit composition. J. Neurosci. *17*, 58–69.

Takamori, S., Rhee, J.S., Rosenmund, C., and Jahn, R. (2000). Identification of a vesicular glutamate transporter that defines a glutamatergic phenotype in neurons. Nature *407*, 189–194.

Thalhammer, A., Morth, T., Strutz, N., and Hollmann, M. (1999). A desensitization-inhibiting mutation in the glutamate binding site of rat alpha-amino-3-hydroxy-5-methyl-4-isoxazole propionic acid receptor subunits is dominant in heteromultimeric complexes. Neurosci. Lett. *277*, 161–164.

Traynelis, S.F., Silver, R.A., and Cull-Candy, S.G. (1993). Estimated conductance of glutamate receptor channels activated during EPSCs at the cerebellar mossy fiber-granule cell synapse. Neuron *11*, 279–289.

Trussell, L.O. (1999). Synaptic mechanisms for coding timing in auditory neurons. Annu. Rev. Physiol. *61*, 477–496.

Tu, L., and Deutsch, C. (1999). Evidence for dimerization of dimers in K+ channel assembly. Biophys. J. *76*, 2004–2017.

Verdoorn, T.A., Burnashev, N., Monyer, H., Seeburg, P.H., and Sakmann, B. (1991). Structural determinants of ion flow through recombinant glutamate receptor channels. Science *252*, 1715–1718.

Washburn, M.S., Numberger, M., Zhang, S., and Dingledine, R. (1997). Differential dependence on GluR2 expression of three characteristic features of AMPA receptors. J. Neurosci. *17*, 9393–9406.

Wenthold, R.J., Petralia, R.S., Blahos, J., II, and Niedzielski, A.S. (1996). Evidence for multiple AMPA receptor complexes in hippocampal CA1/CA2 neurons. J. Neurosci. *16*, 1982–1989.

Yamada, K.A., and Tang, C.M. (1993). Benzothiadiazides inhibit rapid glutamate receptor desensitization and enhance glutamatergic synaptic currents. J. Neurosci. *13*, 3904–3915.